Liu *et al. Geoscience Letters* (2022) 9:17
https://doi.org/10.1186/s40562-022-00229-8

Geoscience Letters

RESEARCH LETTER

Open Access

A pixel analysis technique and unmanned aircraft system for horizontal displacement in the landslide potential area

Che-Hsin Liu[1], Jui-Yi Ho[1*], Chung-Ray Chu[1], Chih-Hsin Chang[1] and Hongey Chen[1,2]

Abstract

Quantitative horizontal displacement in the landslide potential area is necessary for mitigating casualties, property damage, and economic loss. Focusing on a sliding within a deep-seated landslide potential area located in Guanghua area in northern Taiwan, this study employed an unmanned aerial system (UAS) to capture and produce seven high-precision orthomosaics from February 23 to March 26, 2021. Through particle image velocimetry (PIV) method, these orthomosaics were used to assess the two-dimensional land surface displacement in the sliding-movement region. The results revealed substantial displacement in the study region within the monitoring period. The direction of displacement was consistent with the slope aspect in the region. To evaluate the suitability of the proposed model, the coefficient of efficiency was chosen to determine the goodness-of-fit between the observed and calculated two-dimensional displacement in situ land surface displacement extensometer. The result showed that coefficient of efficiency was up to 0.998. In addition, the greatest displacement was observed in the vegetated section located at the bottom of the sliding-movement region. This section also had the highest slope, and its maximum tree-crow displacement exceeded 9 m. PIV facilitated easy identification of the range and boundaries of the sliding area. This noncontact monitoring technique overcame the limitations of single-point displacement assessment, obviating the time-consuming, costly processes involved in conventional monitoring methods. The achieved results obtained by proposed method gave a worthy support for an accurate understanding and evaluation of the landslide processes in the watershed. The technique can also be applied to other critical infrastructure sites, allowing hazard risk reduction.

Keywords: Large-scale landslide, Unmanned aerial system (UAS), Particle image velocimetry (PIV), Land surface displacement

Introduction

Taiwan has a high landslide potential because of its climate, location on the active boundary between Eurasian Plate and Philippine Sea Plate, topography with more mountains than plains predominated by mountains, as well as seasonal rains and typhoons. For instance, the heavy rainfall that came with Typhoon Morakot in 2009 caused landslides in various mountainous areas in Central and Southern Taiwan. Landslides affect the configuration of land surfaces, making it a main factor that contributes to land erosion. Various types of landslides have resulted in substantial mortality and socioeconomic damage (Chen 2000; Chen et al. 2006, 2020; USGS 2004). The hazard of such slope disasters can be assessed before they actually occur by using several survey techniques or monitoring the history of slope disasters in the particular area. This includes collecting and interpreting remote sensing images, investigating and testing the hydrological and geological characteristics, analyzing the slope stability, or installing different types of monitoring instruments (Chung et al. 2016).

*Correspondence: juiyiho@ncdr.nat.gov.tw

[1] National Science and Technology Center for Disaster Reduction, New Taipei City 23143, Taiwan
Full list of author information is available at the end of the article

However, slope stability analysis and hydrological and geological surveying both require a large amount of diverse, long-term in situ survey data—which leads to increased costs, discontinuous survey stations, and difficulties in conducting surveys in multiple areas. Accordingly, remote sensing imaging techniques have been commonly used to support in situ analysis, potential assessment, and monitoring of slope disasters.

Unmanned aircraft system (UAS) integrated with an aerial photography system for nonmetric cameras, which is an aerial photography system that quickly captures spatial information of land surfaces, has been developed recently (Gomez and Purdie 2016; Greenword et al. 2020). This aerial photography system is flexible and quick and can function under low clouds. Compared with conventional aerial remote sensing imaging, this new aerial photography system is less susceptible to cloud conditions, more portable, more flexible, and of lower cost. It also acquires image data of disaster areas more quickly and thus facilitates smooth rescue operations in disasters (Karantanellis et al. 2020; Conforti et al. 2021; Ybanez et al. 2021).

Building on a UAS, this study produced multiperiod high-resolution orthomosaics for the study area and employed particle image velocimetry (PIV) to assess land surface displacement in the study landslide area. In the past, PIV was mostly applied in indoor fluid mechanics experiments or in situ flow field observations; the particle images in flow fields captured with a high-speed or fixed camera were used to analyze the amount of deformation and estimate the velocity field of fluids. The relationships between precision, accuracy, and resolution of the analysis results were clarified in a stepwise manner during the analysis (Adrian 1991; White et al. 2003; Baba et al. 2012; Daigle et al. 2013). PIV has also been applied in various indoor mechanical tests for rock fractures and case studies of landslides in Taiwan. For instance, PIV has been used in a physical model that simulates land surface materials on a fault plane to observe the relative lateral and rotational movements in the displacement field and thus delineate the cracks. Land surface displacement analysis has been conducted for landslides occurring in various areas (Tseng et al. 2009). These studies have used multiperiod orthoimages to assess land surface displacement at various time points; established an analysis procedure for estimating the amount of displacement; discussed the sources of error in orthoimages, including aerial photography equipment and time-variable factors such as shadows, vegetation, and seasons; and explored how post-processing and filtering

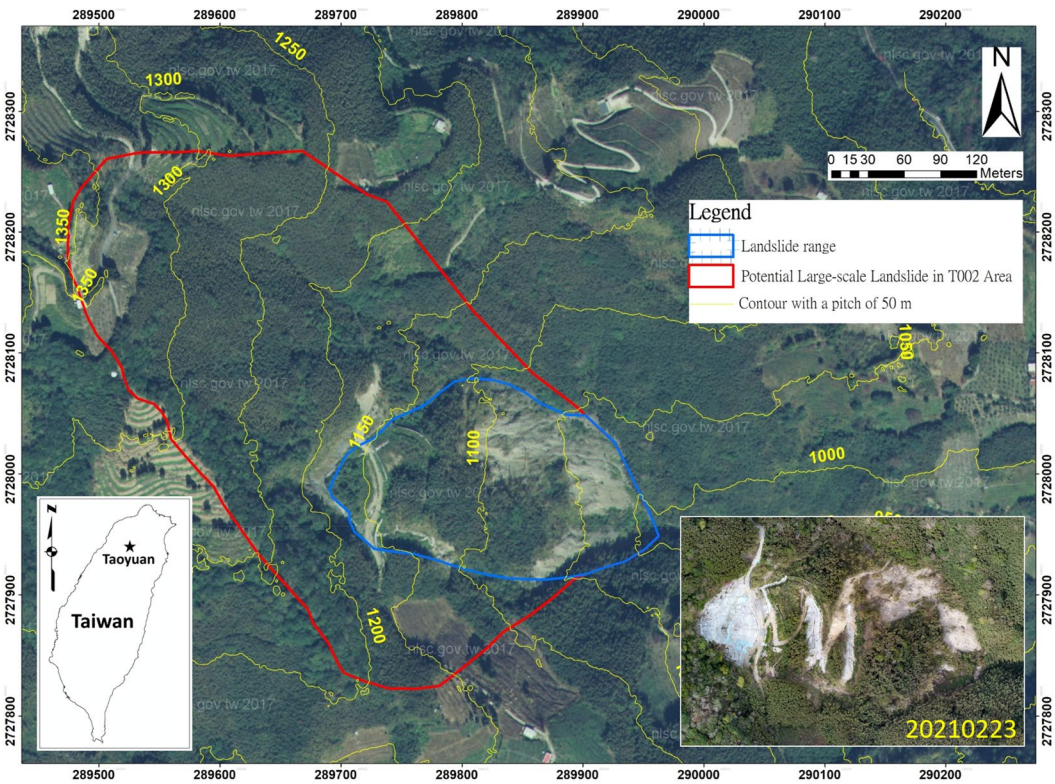

Fig. 1 Location maps of the study regions

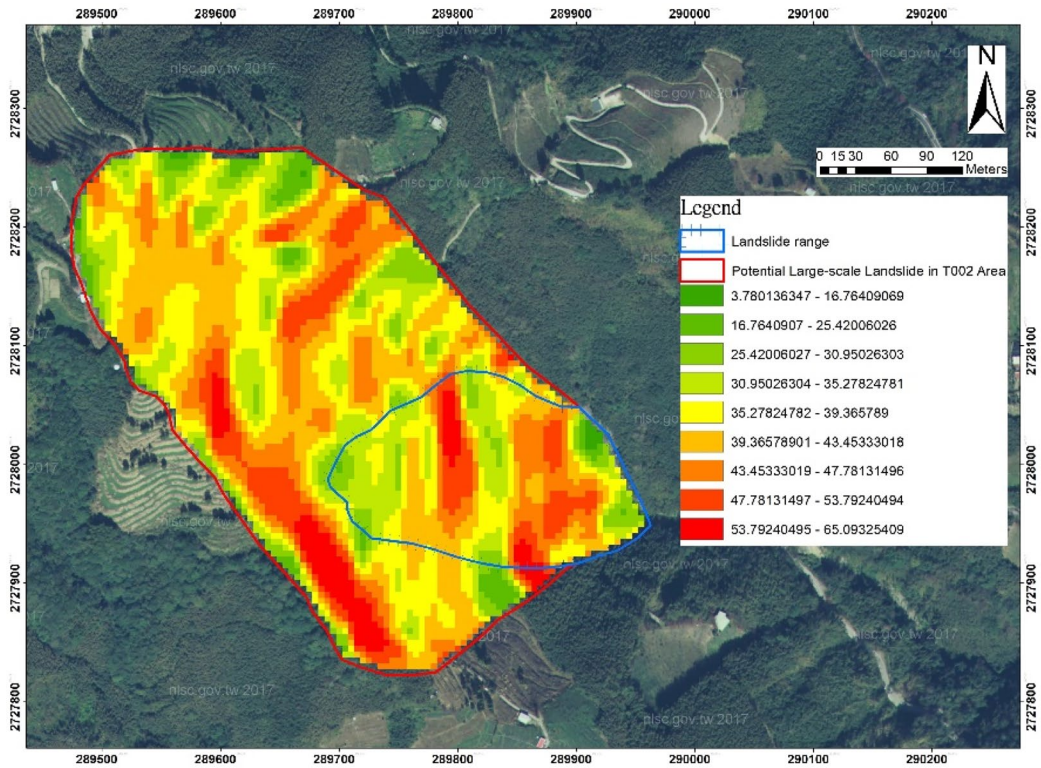

Fig. 2 Slope of the study region

techniques could be used to test parameter relevance and reduce the influence of error.

As shown above, applying PIV in land surface displacement analysis is a mature practice in research. However, in the past, orthoimages were generated using data captured through aerial photography with manned aircrafts. Images captured with manned aircrafts have a relatively high resolution, attributable to the high flying height, large swath width, and large photographic coverage; however, the elevation error can easily lead to distorted orthoimages. Accordingly, producing appropriate image data for PIV analysis is difficult. The recent rapid development of UAS has facilitated the collection of high-precision images through aerial photography. This study integrated the UAS with PIV to ensure that adequate land surface displacement information could be obtained from the high-resolution aerial image data; the information included the scale, direction, and amount of displacement. The integrated approach may have a wide application to the assessment of land surface deformation.

Study area

The study area was a large-scale landslide potential area in the Guanghua region in Fuxing District, Taoyuan City; the area is coded Taoyuan City-Fuxing District-T002 by the Soil and Water Conservation Bureau in Taiwan. This landslide potential area had an area of 12.4 ha (circled in red in Fig. 1), and the actual scale of the sliding area was appropriately 3.1 ha (circled in blue in Fig. 1). In the sliding-movement region, the sliding started in 2002 and has been accelerating since January 2021. A landslide, if it occurs, would directly affect people and properties in the landslide area, which include those on the farm road, and increase sediment deposition and undermine water quality in reservoirs. Land surface displacement was only noticeable in the sliding-movement region, and no signs of sliding were observed in the remainder of the landslide potential area. Figures 2, 3 are the slope and aspect maps of the sliding-movement region before the movement accelerated produced using a 5-m-resolution digital elevation model, respectively. According to the slope map,

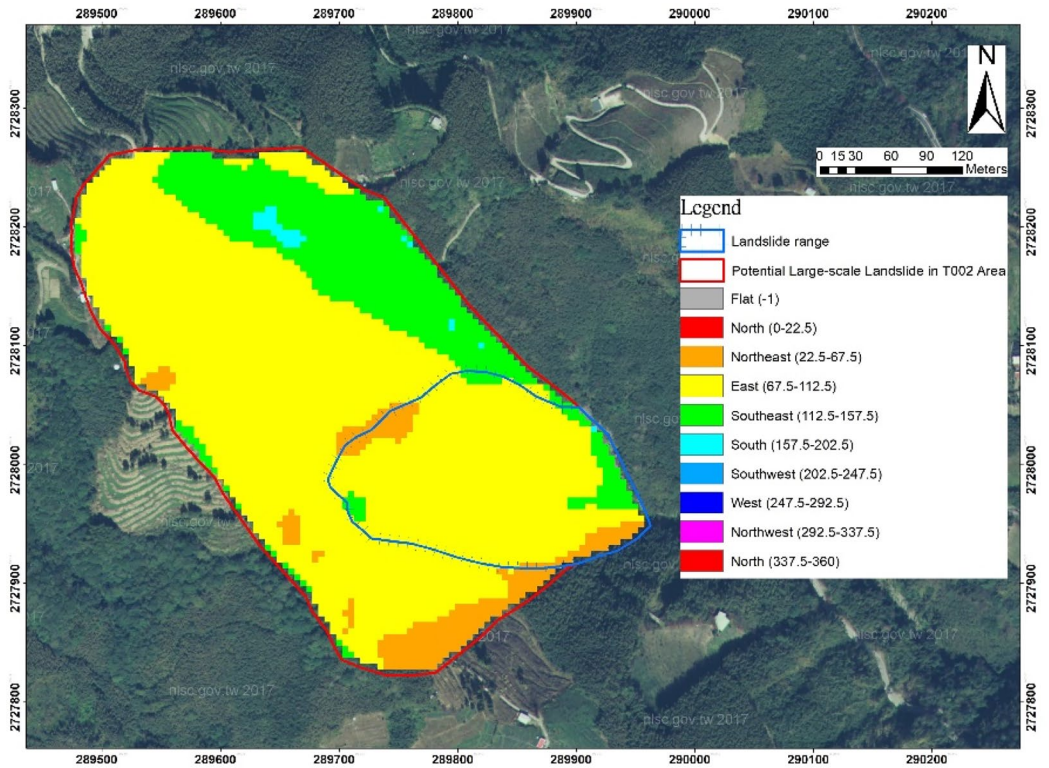

Fig. 3 Aspect of the study region

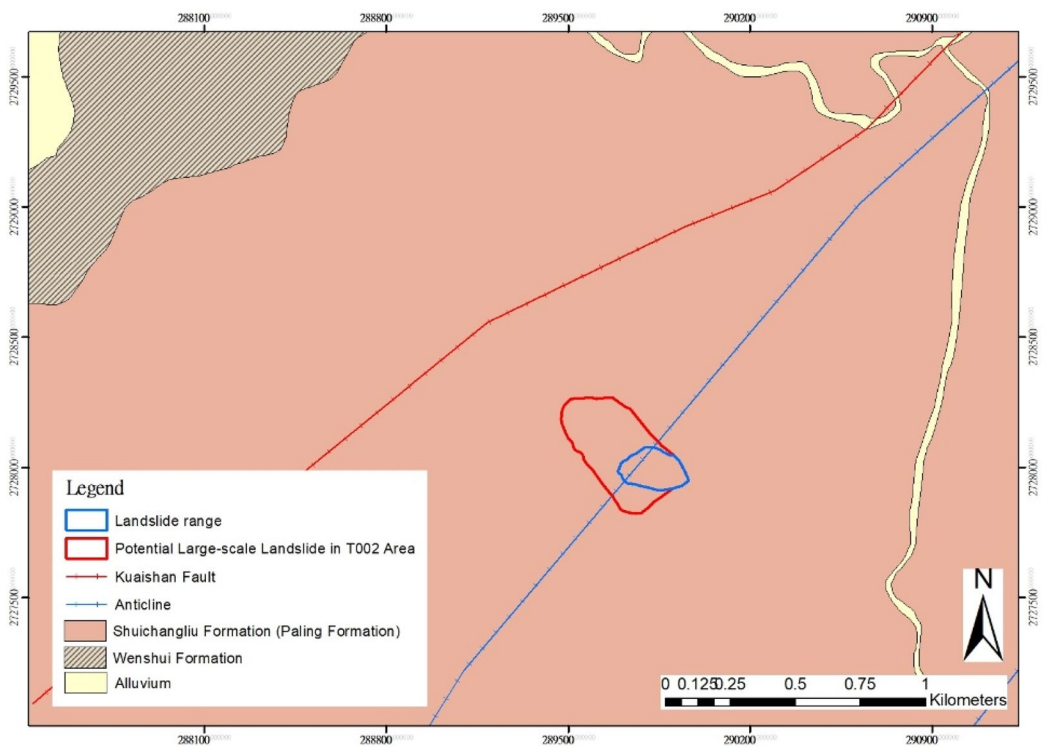

Fig. 4 Geology of the study region

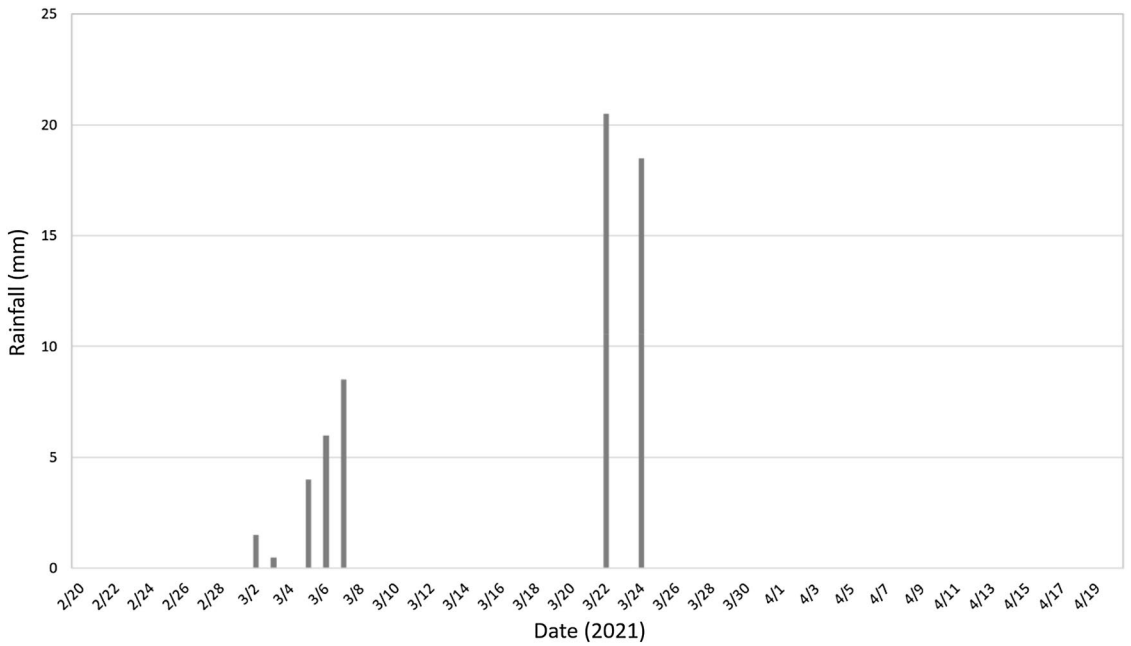

Fig. 5 The daily rainfall records from 2/20 to 4/19 in the study area

Fig. 6 The groundwater flow exfiltration in the study area

the vegetated section, located in the lower part of the sliding region, is relatively steep. The aspect map shows that all the slopes face eastward. This information could all be used to verify the results of the subsequent land displacement analysis.

Regarding the geology of the large-scale landslide potential area, the predominant stratum is the Paling formation—which features mainly dark-gray to gray argillite and slate, and occasionally, a thin layer of gray, fine, and argillic sandstone in the lower part of the stratum. An interlaced layer structure can occasionally occur in the sandstone layer. The fragments created through weathering are in round or pencil-like shapes. The geological structure near the study area comprises mainly an unnamed anticline and the Kuaishan Fault, located 80 m to the east of the large-scale landslide potential area and oriented in the northeast–southwest direction. The upper and lower blocks of the Kuaishan Fault are all composed of the Paling formation. According to 1/50,000 geological map of Taiwan (Fig. 4), an unnamed anticline seems to traverse the study area. However, the measured attitude of the anticline suggested that the anticline is distant from the Guanghua region, and the measured outcrop attitude also showed that the anticline does not travel through the study area.

Landslides belong to the most important natural hazards in all mountainous regions. It is well known that water is one of the major triggers of landslides. Numerous landslide studies discuss different effects that water

location	N	E	H	2DCQ (m)	3DCQ (m)
GS01	2727934.495	290075.686	943.964	0.0066	0.0187
GS02	2727955.544	290223.663	953.164	0.0061	0.0186
GS03	2728250.002	289531.045	1320.367	0.0087	0.0232
GS04	2728198.694	289513.780	1332.095	0.0104	0.0308

Fig. 7 Locations of ground control points and the coordinates and precision of TWD97

may have on slope stability: decreasing suction, rising groundwater table and subsequent increasing pore water pressure, groundwater exfiltration from the bedrock, seepage erosion, hydraulic uplift pressure from below the landslide. Figure 5 shows the daily rainfall records from 2/20 to 4/19 and only few accumulated rainfall in the study area (annual rainfall is up to 3000 mm). According to results obtained from terrain surveys, geological boring, and monitoring coupled with subsurface data retrieved during the collecting conduit operation, the landslide mechanism was preliminarily determined to be the following factors (which contributed to slope instability): deposition of a thick layer of regolith on the slope surface, broken rocks at several depths of the rock formation, high-angle cracks, multiple slide depths, the exposed toe area's susceptibility to environmental conditions and instability, and the flow characteristics and complexity of the regional groundwater. The predominant landslide type is regolith slides, which occur at approximately 5–27 m below the land surface (Soil and Water Conservation Bureau in Taiwan 2021). As shown in Fig. 6, the groundwater was exfiltration on the slope

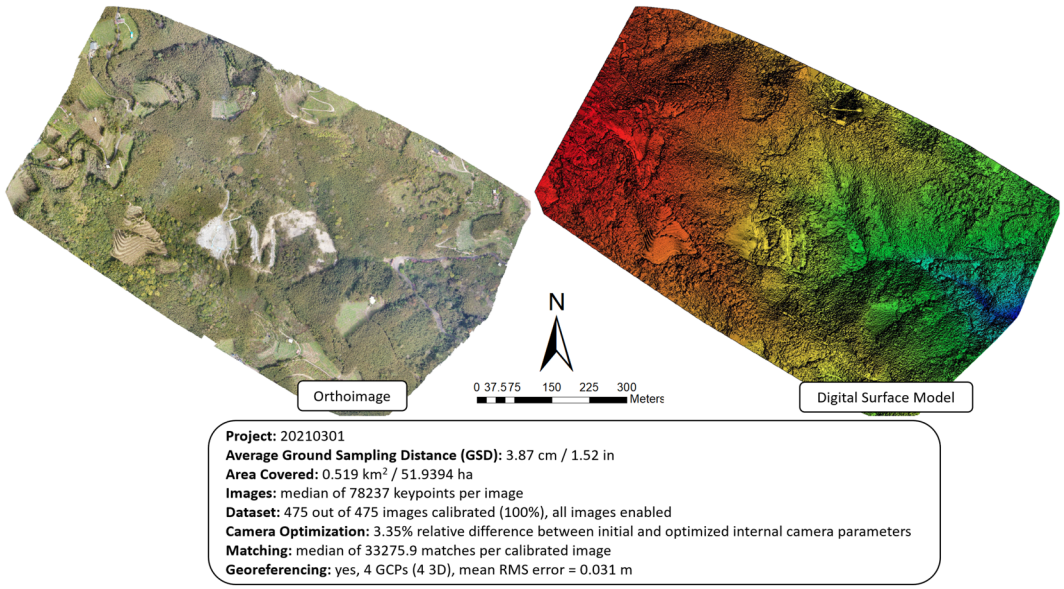

Fig. 8 Orthomosaic and the corresponding sparse digital surface model (DSM)

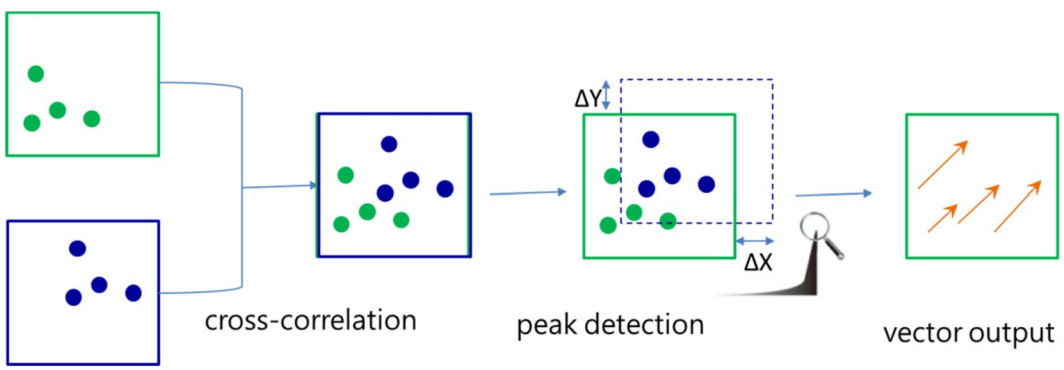

Fig. 9 Procedure of PIV's analysis

in the study area. The regional groundwater flow exfiltration may be the major trigger of the landslide in the study area.

Methodology

This study employed PIV to analyze the land surface displacement of a landslide. The analysis procedure was as follows: using an UAS to capture orthoimages of the study area; identifying appropriate ground control points within the area; use high-precision satellite positioning devices to obtain the three-dimensional coordinates of the ground control points; and inputting the high-resolution coordinate data when producing the orthomosaics to enhance the overall precision of the orthomosaics. Through this procedure, multiperiod orthomosaics were obtained and analyzed using PIV to calculate the land surface displacement at various periods. The subsequent paragraphs detail on the tasks involved at each stage of the procedure.

For producing orthomosaics, the authors ensured that the entire large-scale landslide potential area was covered in the images. Four ground control points were selected outside the main sliding area, where coordinate and elevation data were collected using high-precision satellite positioning devices (Fig. 7). The unmanned aerial vehicle was installed with a 24-million-pixel camera for capturing images and flew at 150 m. An image captured had an 85% overlap with the ones above and below it and a 70% overlap with the one to the left and right of it. The captured images were subject to matching, mosaicking,

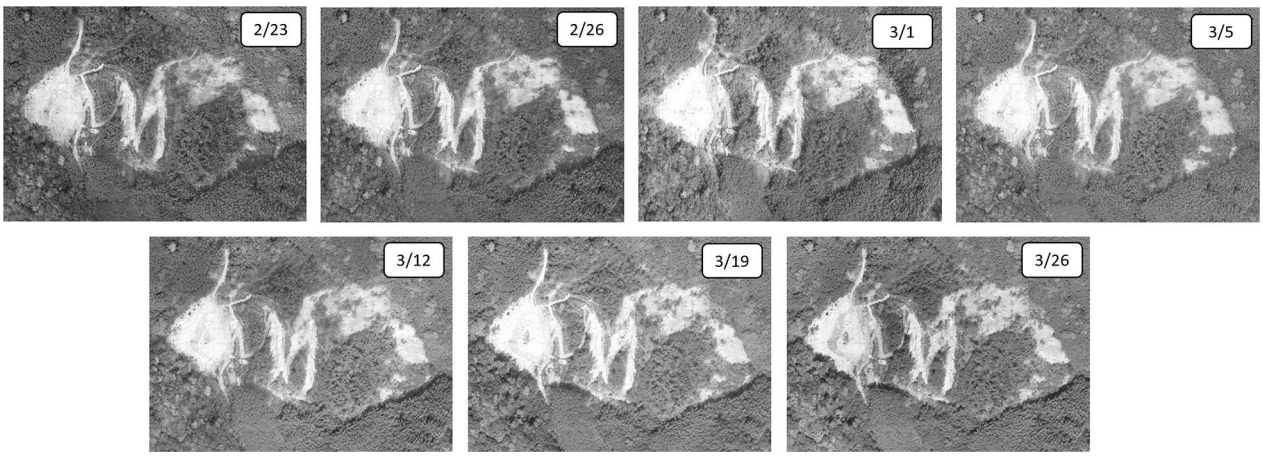

Fig. 10 Grayscale images of different periods

Fig. 11 PIV evaluation setup in the study area

aerial triangulation, and point cloud densification in Pix4D mapper pro to produce orthomosaics and digital surface model data (Fig. 8). Following the aforementioned steps, the authors could maintain a precision of ≥ 10 cm in the average ground sampling distance and ground control points.

The obtained multiperiod orthomosaics were used to analyze the land surface displacement in the landslide area on PIVview2C (version 3.6; PIVTEC). Figure 9 presents the mechanics of the software. First, an image is fixed and compared with another one to obtain the relative displacement. Comparison and correlation calculations were performed on similar pixels to detect the peak correlation coefficient. The coefficient indicates the vector field in which the two images' particle features can be mutually superimposed and are completely matching, and the correlation offset is identical to the displacement. These steps were taken to identify the mean displacement of particles and thus understand the overall particle movement in the environment (PIVTEC GMBH 2015).

After images of two periods are imported to the software program, several critical parameter settings are required before the horizontal displacement analysis can be started. First, the first image was divided into a mesh of test patches with the same size; the amount of two-dimensional displacement of each test patch mesh was obtained after its analysis was complete. For calculating the amount of displacement between the test

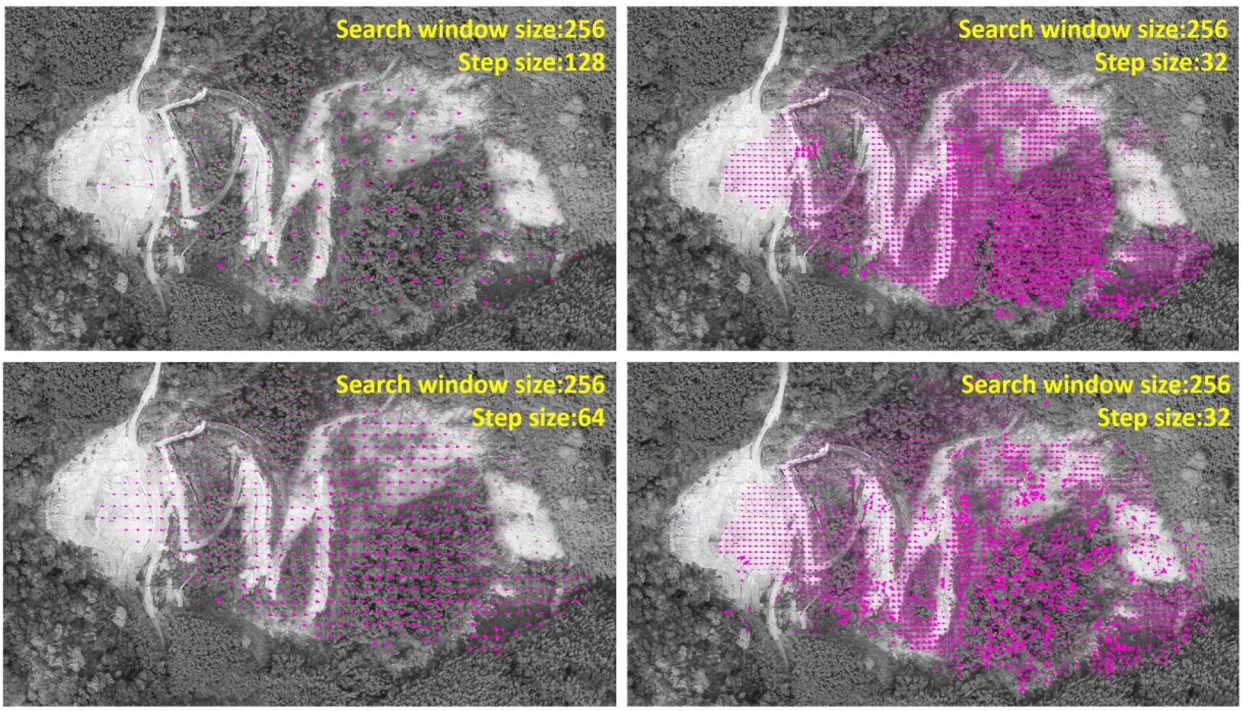

Fig. 12 The testing of the PIV's window size and step size

patches in two images, the size of search patch was set in another image; the search zone was determined to be the area of the maximum test patch movement in relation to the two directions in a two-dimensional space. A larger patch encompasses a greater number of image features and hence provides more precise results. However, a fixed-size image provides few measurement points for displacement calculation, making window size and step size of the search patch two critical parameter settings that require testing.

Search patches with identical coordinates in two images were subject to cross-correlation to determine the level of correlation between the two images. The cross-correlation analysis were performed using the following equation:

$$C(s)=\int\int W^{'}(x)I^{'}(x)W^{''}(x+s)I^{''}(x+s)\mathrm{d}x, \quad (1)$$

where C(s) is the level of correlation; $I^{'}$ and $I^{''}$ are the window size of search patches; $W^{'}$ and $W^{''}$ are the image files of the first and second images, respectively; and s is the amount of displacement between the two images. Using search patches of varying sizes could directly undermine the precision of analysis results. The relationship between error and search window size is expressed as follows:

$$\rho_{pixel} = 0.6/L + 150000/L^{8}, \quad (2)$$

where L is the search window size and ρ_{pixel} is the standard error.

According to the literature, the larger the search patch, the more precise is the analysis results but the fewer are the obtained measurement points. Moreover, the analysis precision decreases if the amount of image displacement is not an integer multiple of the number of image pixels. In addition to window size and distance of movement, the image feature points are a primary factor affecting the analysis results. Image features are variable across times and seasons, such as vegetation; for buildings and construction structures, their features may change with the lighting and shadow conditions at the time of shooting. In situations where the study area is large and a low correlation is observed in the image analysis, valley or shadow areas can be excluded in the subsequent analyses because the surface features of valleys are highly variable, and shadowed features cannot be identified. Subjecting images to grayscale processing and equating the grayscale distribution before PIV analysis can effectively increase the matching correlation coefficient of non-shadowed areas. These are all the crucial factors affecting the result of PIV analysis (White et al. 2003; Tseng et al. 2009).

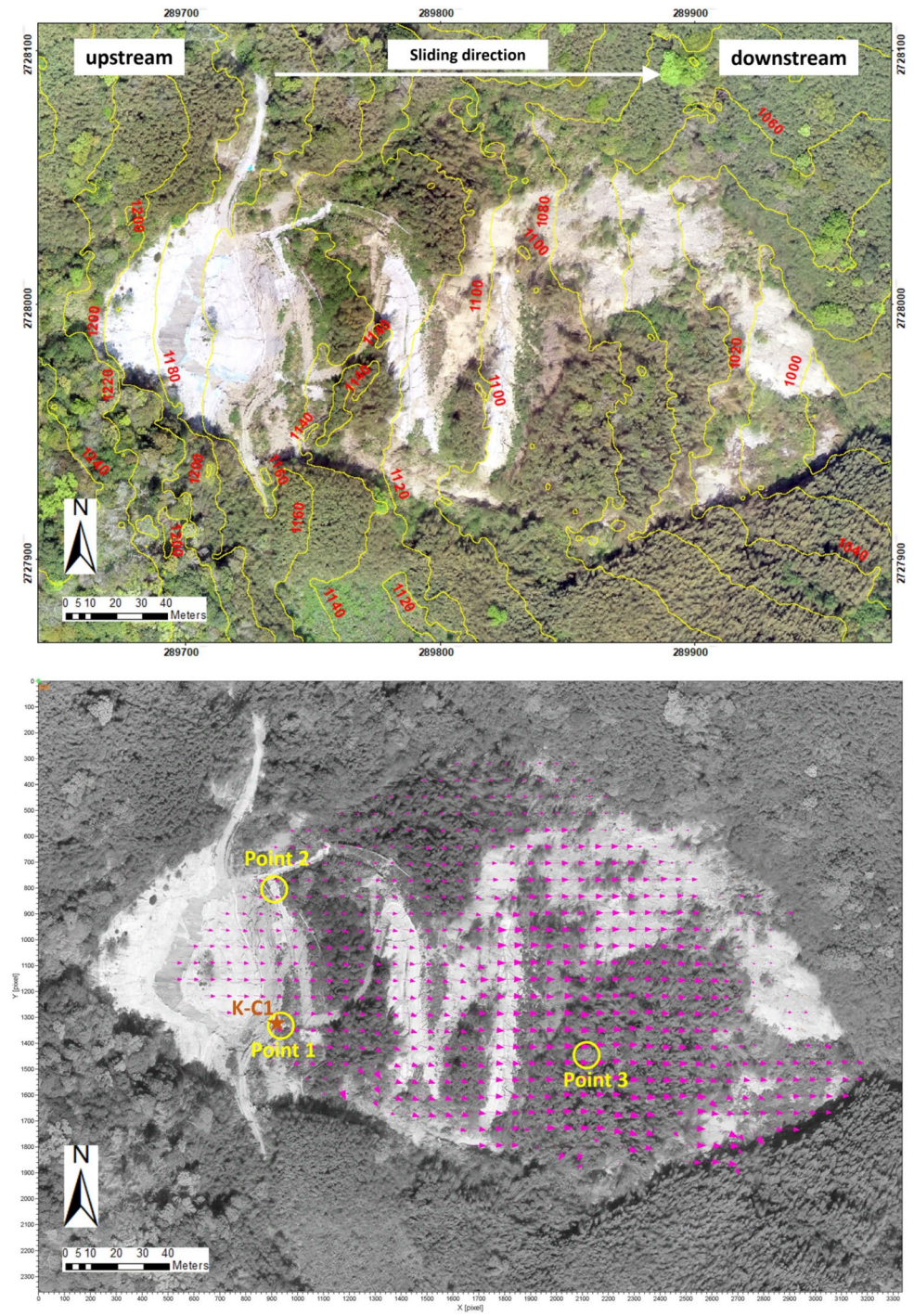

Fig. 13 PIV displacement analysis results for orthomosaics captured on February 23 and March26

In comparing the differences between orthomosaics of different periods, the orthomosaics were cropped to the same photographic coverage and adjusted to the same level of resolution, with the effect of color minimized, to facilitate the analysis and comparison of land surface displacement under identical standards. Seven orthomosaics from the period of February 23 to March 26, 2021, were selected, cropped to the same photographic coverage, adjusted to the same level of resolution (10 cm/pixel), and processed using grayscale equation before

Table 1 Displacement values collected by K-C1 and calculated for reference points (unit: mm)

Time	K-C1	Point 1	Point 2	Point 3
2/23 (12:00)	500	600	535	1436
3/01 (12:00)	1111	1109	916	2591
3/05 (12:00)	1801	2009	1660	4008
3/12 (12:00)	3222	3422	2612	6225
3/19 (12:00)	4390	4330	3174	7761
3/26 (12:00)	5366	5515	4101	9214
CE		0.998	0.917	0.793

$CE = 1 - \sum_{t=1}^{n} (D_{rec}(t) - D_{cal}(t))^2 / \sum_{t=1}^{n} (D_{rec}(t) - \overline{D}_{rec})^2$, where $D_{rec}(t)$ and $D_{cal}(t)$ denote the recorded and calculated displacement at time t, respectively; $\overline{D}_{rec}$ is the mean recorded displacement, and n is the number of displacement records. The CE is used to measure the similarity between the calculated and observed displacements. A more accurate fit is obtained when the value of CE is approximately one

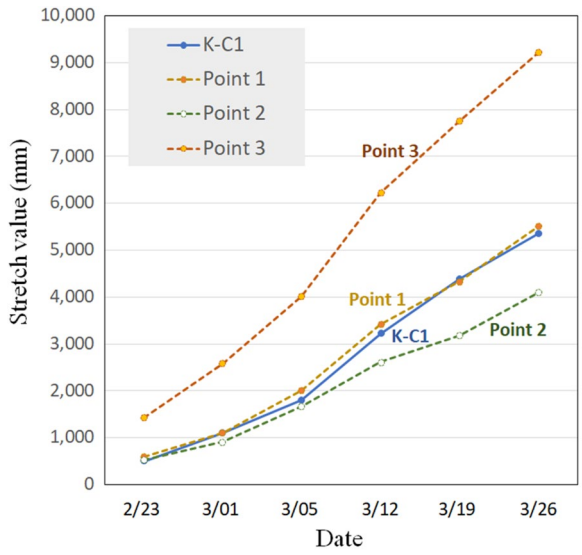

Fig. 14 Monitoring results by K-C1

further analyses were conducted (Fig. 10). According to the PIV user's manual (2010), the interrogation window size is the rectangular size with which the PIV images are sampled to perform the local cross-correlation analysis. Frequently the interrogation window is also referred to as interrogation spot. The window dimensions can be freely set. Because the study area size is only 3335×2359 pixels (333.5×235.9 m), the search window size is set 256 pixels (25.6 m) which is less than the study area (Fig. 11). Step size defines the increment with which the images are sampled. These values define the mesh size of the final data size. Typical values are around 50% of the window size which satisfies the sampling criterion. Greater sample overlap (e.g., smaller step sizes) produces oversampled data, but does not necessarily yield additional information. Consequently, the step size is set 128 pixels (12.8 m), 64 pixels (6.4 m), and 32 pixels (3.2 m) to calibrate the best step size. The detailed results are shown in Fig. 12, when the step size is set large pixels (128 pixels) could not provide the representative slide movement with highly precision in the study area. When the step size is set as small pixels (32 pixels), only few feature points can be found. If the step size is greater than or close to the local horizontal displacement in the study area, some error results such as the error direction of sliding would occur. Through testing, the PIV search window size and step size for two-dimensional displacement of land surface analysis were determined to be 256 and 64 pixels, respectively.

Results and discussion

Seven orthomosaics of the sliding-movement region in the Taoyuan City-Fuxing District-T002 large-scale landslide potential area captured between February 23 and March 26, 2021, were used for PIV analysis so as to calculate the land surface displacement in the region. Figure 13 presents the analysis results of orthomosaics captured on February 23 and March 26 (31 days apart). The red arrow indicates the amount and direction of displacement obtained through analysis. The larger arrows mean the grid is with large displacement. Accordingly, the scale and boundaries of the displacement areas as well as the amount and direction of sliding can be identified easily through Fig. 13. A comparison with the aspect map in Fig. 3 revealed that the direction of displacement in the sliding-movement region was consistent with the slope aspect. Notably, the aforementioned result was generated using orthomosaics in PIV; in other words, the calculated displacement was two-dimensional, and thus, the slope must be considered if it is to be compared with the in situ monitoring result.

Three reference locations (Points 1–3 in Fig. 13) in the sliding area were selected to explain the actual land surface displacement values. The reason Point 1 was chosen was that this location was close to the monitoring point of the Soil and Water Conservation Bureau's in situ land surface displacement extensometer K-C1, facilitating comparison with the in situ monitoring values. Points 2 and 3—the least and most displaced locations, respectively—were selected for observing the PIV analysis results. Point 3 was selected to explore the largest amount of displacement within this area during the study period because it was located at the top of the tree crowns in the vegetated section. Table 1 lists the displacement values for the three reference locations (points) calculated through PIV and collected in situ by K-C1 was considered in the calculation of these values, and thus, the

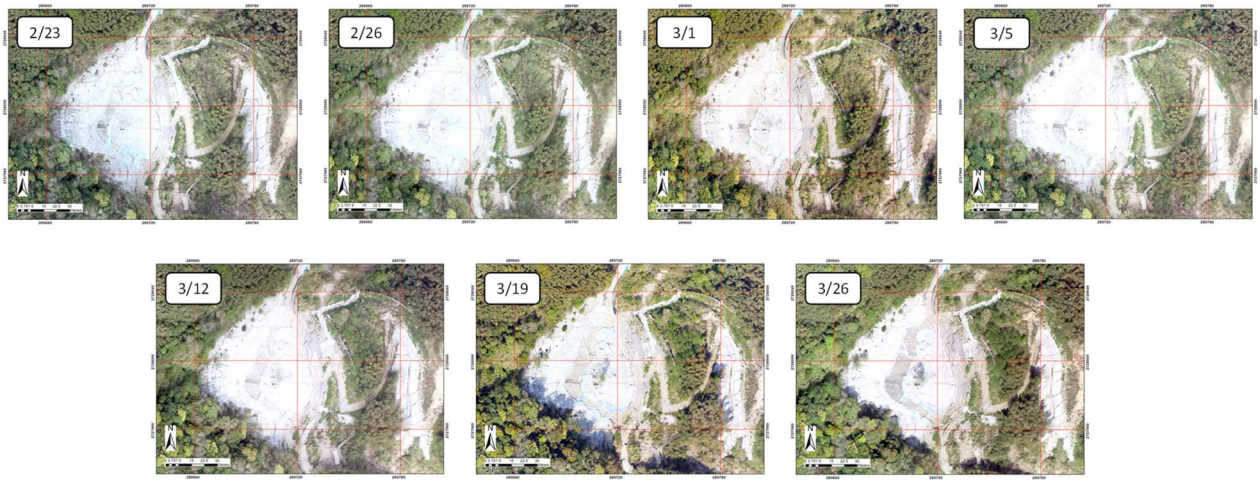

Fig. 15 Comparison of the top region of the sliding-movement region in orthomosaics

calculated values for Point 1 could be directly compared with those collected by K-C1. The quantitative relationship by analyzing the correlation between the K-C1 point and the calculated three-point data are presented in Table 1. To evaluate the suitability of the proposed model, the coefficient of efficiency (CE) was chosen to determine the goodness-of-fit between the observed and calculated two-dimensional displacement in the K-C1 Point. The results showed that coefficient of efficiency (CE) is up to 0.998 at Point 1, 0.917 at Point 2, and 0.793 at Point 3. Because the Point 1 is very close to K-C1 point shown in Fig. 14, indicating that the calculated and recorded displacements are in excellent agreement. The results also shown that the displacement at downstream (Point 3) is significantly large than the displacement at the upstream (Point 1), and the displacement at Point 1 is large than the displacement at Point 2. The proposed noncontact monitoring technique (PIV with UAS) provided the two-dimensional land surface displacement in the all landslide potential area with highly precision that overcame the limitations of single-point displacement assessment (K-C1), obviating the time-consuming, costly processes involved in conventional monitoring methods.

Figure 15 compares the top region of the sliding-movement region captured in the orthomosaics on February 23 and March 26 and shows considerable displacement in the sliding during the 31-day period. Figure 16 depicts the land surface displacement analysis results obtained using the seven orthomosaics captured at different periods. The largest displacement occurred at the vegetated section located at the bottom of the sliding region; this section, as shown in Fig. 2, had a relatively steep slope, and thus, the amount of land surface displacement in this section would naturally be greater than that in other parts of the area. In addition, the amount of displacement appeared to be even greater when observed from the tree crowns.

Conclusion

With the Taoyuan City-Fuxing District-T002 (Guanghua) large-scale landslide potential area as the study area, the present study employed a UAS to capture and produce seven high-resolution orthomosaics between February 23 and March 26, 2021. PIV was performed to assess the two-dimensional land surface displacement in the study area. The results reveal substantial land surface displacement in the sliding-movement region during the 31-day period; the direction of displacement was consistent with the aspect of slope in this region, and the amount of displacement was close to that monitored in situ. The greatest displacement occurred at the vegetated section located at the bottom of the sliding-movement region. This section also had the steepest slope in the region, and its maximum amount of tree-crown displacement exceeded 9 m.

Most studies employing PIV have employed a large study area and used manned aircrafts to capture orthoimages; the flying height was usually high and thus produced much elevation error to be calibrated. In addition, for image data collected in different periods, the shooting time intervals were long, and the image quality was highly susceptible to the vegetation or lighting conditions in different seasons. The various sources of orthoimages and large variance in image resolution resulted in the relatively low correlation coefficients in the PIV analysis. This, in turn, required an additional filtering step to filter out unreasonable vector

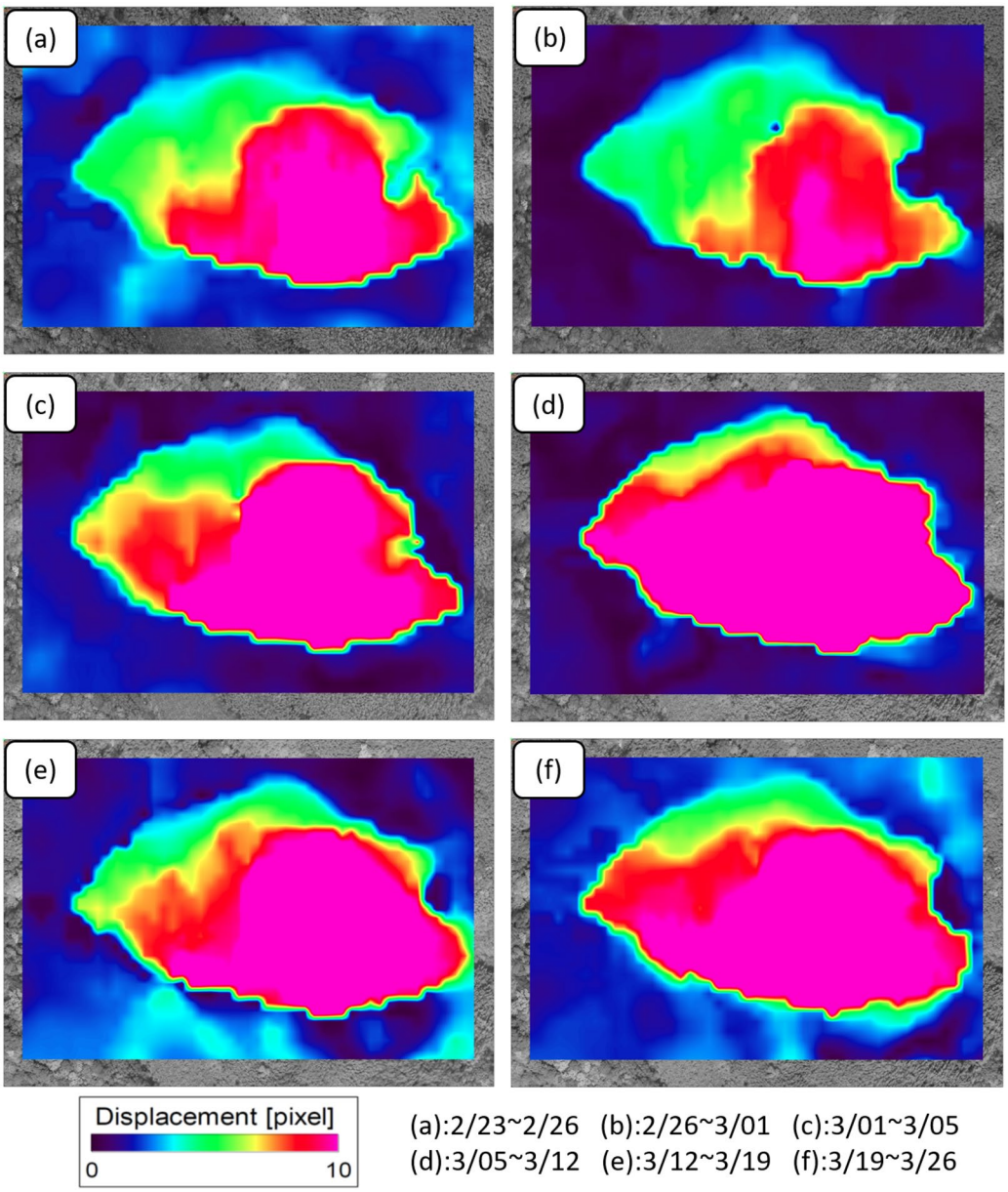

Fig. 16 Color gradient map of the PIV displacement analysis results for the study period

displacement results before establishing the displacement field of the study area, followed by a comparison between the slope aspect, feature points, and terrain cross-section to verify the analysis results. The present study area was relatively small, and the orthoimages were captured using a multirotor unmanned aerial vehicle, the flying height of which was lower than that of conventional manned aircrafts and thus produced low elevation error but high resolution and high precision. Furthermore, the shooting time intervals for the seven orthomosaics were short; the shooting times were fixed in the period between 11:00 to 13:00 to minimize the influence of seasons and shadow; and the slope aspect was consistent in the study area. These characteristics of the present study were all conducive to PIV assessment of land surface displacement in the sliding-movement region. The PIV technique is a useful tool for accessing two-dimensional displacement of land surface, and has been used in various indoor experiments in channels with constant slope. Based on the mature technique of UAS and PIV, we think that third parties through the same process can reproduce the results of the land surface displacement due to a sliding in a field.

Acknowledgements
This research was supported by the Soil and Water Conservation Bureau, Taiwan, under Grant SWCB-109-227. The authors acknowledge the financial support provided by the Ministry of Science and Technology.

Author contributions
CL, JH, and CC validated the proposed model. CC and HC designed and performed the model. All authors contributed about equally to compose this paper, discussed the results, and commented on the manuscript at all stages. All authors read and approved the final manuscript.

Availability of data and materials
Vs data will be shared through the Soil and Water Conservation Bureau, Taiwan, after this paper is published.

Declarations

Ethics approval and consent to participate
The authors would like to confirm that they have no competing interest regarding this paper. All authors worked closely on this project starting from the conception of the project through modeling, analysis, interpretation of the results and write-up of the manuscript.

Competing interests
The authors declare that they have no competing interests.

Author details
[1]National Science and Technology Center for Disaster Reduction, New Taipei City 23143, Taiwan. [2]Department of Geosciences, National Taiwan University, Taipei 10617, Taiwan.

Received: 28 November 2021 Accepted: 24 April 2022
Published online: 09 May 2022

References

Adrian RJ (1991) Particle imagine techniques for experimental fluid mechanics. Ann Rev Fluid Mech 23:261–304
Baba HO, Peth S (2012) Large scale soil box test to investigate soil deformation and creep movement on slopes by particle image velocimetry (PIV). Soil Tillage Res 125:38–43
Chen H (2000) Engineering geological characteristics of Taiwan landslides. Sino Geotech 79:59–70
Chen H, Dadson S, Chi YG (2006) Recent rainfall-induced landslides and debris flow in northern Taiwan. Geomorphology 77:112–125
Chen L-K, Chang C-H, Lin C-H, Ho J-Y (2020) Application of a three-dimensional deterministic model to assess potential landslides, a case study: antong hot spring area in Hualien. Taiwan Water 12(2):480
Chung M-L, Chen C-H, Lee C-F, Huang W-K, Tan C-H (2016) Investigation and assessment methods for the impact of a largescale landslide on a neighboring village. J Chin Soil Water Conserv 47(3):122–134
Conforti M, Mercuri M, Borrelli L (2021) Morphological changes detection of a large earthflow using archived images, lidar-derived DTM, and UAV-based remote sensing. Remote Sens 13:120
Daigle A, Bérubé F, Bergeron N, Matte P (2013) A methodology based on Particle image velocimetry for river ice velocity measurement. Cold Reg Sci Technol 13:36–47
Gomez C, Purdie H (2016) UAV-based photogrammetry and geocomputing for hazards and disaster risk monitoring—a review. Geoenviron Disast 3(1):23
Greenwood F, Nelson EL, Greenough PG (2020) Flying into the hurricane: A case study of UAV use in damage assessment during the 2017 hurricanes in Texas and Florida. PLoS ONE 15(2):e0227808
Karantanellis E, Marinos V, Vassilakis E, Christaras B (2020) Object-based analysis using 854 Unmanned Aerial Vehicles (UAVs) for site-specific landslide assessment. Remote Sens 12:1711
Nash JE, Sutcliffe JV (1970) River flow forecasting through conceptual models part I—a discussion of principles. J Hydrol 10(3):282–290
PIVview User Manual (2010) PIVVIEW2C/3C Version 3.0, PIVTEC GmbH, Germany
PIVTEC GMBH (2015) PIVVIEW 2C/3C Version3.6 User Manual. PIVTEC GMBH, Germany
Soil and Water Conservation Bureau, Council of Agriculture, Executive Yuan (2021) Response measures report on the Taoyuan City-Fuxing District-T002 (Guanghua) large-scale landslide potential area. Accessed 26 Mar 2021
Tseng C-H, Hu J-C, Chan Y-C, Chu H-T, Lee J-F, Wei J-Y, Lu C-Y, Lin M-L (2009) Non-catastrophic landslides induced by the Mw 7.6 Chi-Chi earthquake in central Taiwan as revealed by PIV analysis. Tectonophysics 466(3):427–437
USGS (2004) Landslide types and processes. Fact sheet 2004–3072. http://pubs.usgs.gov/fs/2004/3072/
White DJ, Take WA, Bolton MD (2003) Soil deformation measurement using particle image velocimetry (PIV) and photogrammetry. Geotechnique 53(7):619–632
Ybanez RL, Ybanez AAB, Lagmay AMFA, Aurelio MA (2021) Imaging ground surface deformations in post disaster settings via small UAVs. Geosci Lett 8:23

Publisher's Note